2013-07-01

Spectral Stability of Weak Detonations in the Majda Model

Jeffrey James Hendricks
Brigham Young University - Provo

Spectral Stability of Weak Detonations in the Majda Model

Jeffrey Hendricks

A thesis submitted to the faculty of
Brigham Young University
in partial fulfillment of the requirements for the degree of

Master of Science

Jeffrey Humpherys, Chair
Chris Grant
Scott Glasgow

Department of Mathematics

Brigham Young University

June 2013

ABSTRACT

Spectral Stability of Weak Detonations in the Majda Model

Jeffrey Hendricks
Department of Mathematics, BYU
Master of Science

Using analytical and numerical Evans-function techniques, we examine the spectral stability of weak-detonation-wave solutions of Majda's scalar model for a reacting gas mixture. We provide a proof of monotonicity of solutions. Using monotonicity we obtain a bound on possible unstable eigenvalues for weak-detonation-wave solutions that improves on the more general bound given by Humpherys, Lyng, and Zumbrun [22]. We use a numerical approximation of the Evans function to search for possible unstable eigenvalues in the bounded region obtained by the energy estimate. For the parameter values tested, our results combined with the result of Lyng, Raoofi, Texier, and Zumbrun [35] demonstrate that these waves are nonlinearly phase-asymptotically orbitally stable throughout the parameter space for which solutions were obtainable.

Keywords: Majda, Evans Function, combustion, shockwave, differential equations

Acknowledgments

First I'd like to thank my advisor, Professor Jeffrey Humpherys for taking time to teach me the skills needed to complete this project. He has also helped provide me with many opportunities to be engaged in a variety of research and other projects which have been of great value to me. I also thank the many other faculty and staff at BYU that have encouraged me along the way.

I also thank Professor Gregory Lyng of the University of Wyoming and Professor Kevin Zumbrun of the University of Indiana whose participation and feedback improved the quality of this work.

Lastly I thank my wife and family for their continuous support of my education.

Contents

Chapter 1. Introduction

1.1 Background: Weak Detonation Waves & Stability

1.1.1 Weak Detonations. In the classical theory of combustion, detonation waves are classified as one of three types: strong, weak, and Chapman–Jouguet [13]. All of these are compressive waves — the pressure and density increase following the wave. We recall that the Chapman–Jouguet detonation is distinguished in the theory. In particular, the CJ detonation travels at the slowest speed of all detonations. Moreover, the point representing the burned state of the CJ detonation separates the detonation branch of the Hugoniot curve into two pieces. The possible burned states on the lower portion of the branch, those corresponding to smaller increases in the pressure, are possible end states for weak detonations. By their nature, these waves occur only rarely if at all [16, 52], and, in contrast to the case of a strong detonation which, like a classical gas-dynamical shock, is supersonic ahead of the front and subsonic behind, in a weak detonation the gas flow relative to the reaction front is subsonic both ahead of and behind the front[1]. This feature makes the stability analysis of such waves delicate. In this paper, we examine the stability of these waves in a simplified combustion model.

In an effort to understand the strongly coupled interaction between the nonlinear motion of a gas mixture and chemical reactions involving the different species of gas making up the mixture, Majda [38] introduced the following "qualitative" model for gas-dynamical combustion

$$(u + qz)_t + f(u)_x = Bu_{xx}\,, \tag{1.1.1a}$$

$$z_t = -k\varphi(u)z\,. \tag{1.1.1b}$$

[1]The CJ detonation is sonic behind the front.

In equation (1.1.1), the unknown function $u = u(x,t)$ is real valued and should be thought of as a stand-in for density, velocity, and temperature; the other unknown $z = z(x,t)$ satisfies $0 \leq z \leq 1$ and measures the fraction by mass of reactant (fuel) in a simple one-step reaction scheme; the flux f is a nonlinear convex function; φ is the ignition function—it turns on the reaction; and k, q, and B are positive constants measuring reaction rate, heat release, and viscosity, respectively. The main result of Majda's analysis [38] is a proof of the existence of strong and weak detonations, particular kinds of traveling waves, for the system (1.1.1). These waves are combustion waves which connect an unburned state ($z = 1$) to a completely burned state ($z = 0$); they are analogues of the corresponding waves in classical combustion theory [13]. Notably, Majda showed that some of the strong detonations feature a "spike" in agreement with the classical theory. More, the proof shows that weak-detonation solutions of (1.1.1) exist only for distinguished values of the parameters. Indeed, Majda's construction is explicit, and it shows that the existence of a heteroclinic orbit corresponding to a weak detonation requires the structurally unstable intersection in the plane of the one-dimensional stable manifold at the unburned state with the one-dimensional stable manifold at the burned state. Here, our focus is on the dynamical stability of these waves as solutions of the evolutionary partial differential equation. We note that these waves are *undercompressive*; that is, from the hyperbolic viewpoint, the "shock" formed by the end states does not satisfy the Lax shock condition due to a deficit of incoming characteristics. This feature affects the stability analysis. Indeed, in contrast to the case of strong detonations which are of Lax type, we know of no stability results for these waves which are based on energy estimates and/or weighted norms. The outgoing characteristic is an obstacle to these methods. By contrast, our approach, based on the Evans function, applies to such undercompressive waves.

1.1.2 Stability. To describe our approach, we denote by L the linear operator obtained by linearizing about the wave in question. Thus, the approximate evolution of a perturbation

v is described by the linear equation $(\partial_t - L)v = 0$. The Evans function, denoted by D, is an analytic function associated with the operator L. Its zeroes λ with $\operatorname{Re}\lambda \geq 0$ correspond to eigenvalues of L. As Proposition 1.1 shows, the spectral information encoded in the zeros of the D can be used to draw conclusions about the nonlinear stability of the wave in question.

Proposition 1.1 (Lyng-Raoofi-Texier-Zumbrun [35])**.** *Under the Evans-function condition*

$$D(\cdot) \text{ has precisely one zero in } \{\operatorname{Re}\lambda \geq 0\} \text{ (necessarily at } \lambda = 0), \tag{$\star$}$$

a strong or weak detonation wave of (2.1.1) *is* $\hat{L}^\infty \to L^p$ *nonlinearly phase-asymptotically orbitally stable, for* $p > 1$*. Here,*

$$\hat{L}^\infty(\mathbb{R}) := \{f \in \mathcal{S}'(\mathbb{R}) \ : \ (1 + |\cdot|)^{3/2} f(\cdot) \in L^\infty(\mathbb{R})\}.$$

Remark. We recall that if X and Y are Banach spaces, a traveling wave $\bar{u}$ is $X \to Y$ *nonlinearly orbitally stable* if, given initial data u_0 close in X such that if $\|\hat{u} - u_0\|_X$ is sufficiently small, there is a phase shift $\delta = \delta(t)$ such that $\|u(\cdot, t) - \bar{u}(\cdot - \delta(t), t)\|_Y \to 0$ as $t \to \infty$. If also $\delta(t)$ converges to a limiting value $\delta(+\infty)$, the wave is *nonlinearly phase-asymptotically orbitally stable.*

The proof of Proposition 1.1 is based on the pointwise Green-function techniques developed by Zumbrun and collaborators; see, *e.g.*, [59]. Briefly, if one is able to obtain sufficient estimates on the Green function $G(x, t; y)$ solving $(\partial_t - L)G = \delta_y$, it is possible to close an iterative argument to establish a result like Proposition 1.1. The main work of [35] is devoted to establishing such bounds under the condition $(\star)$. Thus, our primary purpose here is to locate the unstable zeros (if any) of the Evans function. In this paper we restrict our attention to the case of weak detonations; a parallel Evans-based stability analysis for strong detonations has been done [22]. Because, in all but the most trivial cases, the Evans

function is typically too complex to be computed analytically, our approach is based on the combination of an energy estimate to eliminate the possibility of large unstable zeros and the numerical approximations of the Evans function to deal with the remaining, bounded region of the unstable complex plane. As we describe below, a particular challenge associated with performing Evans-function computations for weak detonation waves is finding the distinguished parameter values for which these waves exist; see §2.3 below for further discussion and more details about this issue.

1.2 Related Work: stability, weighted norms & energy estimates

A number of stability results for the Majda model have been obtained directly by combinations of energy estimates, spectral analysis, and weighted norms. For example, under the assumption that the heat release q is sufficiently small, Liu & Ying [31] established, via energy estimates, the nonlinear stability of strong-detonation solutions of (1.1.1); Ying, Yang, & Zhu [56] later fine-tuned the analysis. In related work, Ying, Yang, & Zhu [55] extended the small-q nonlinear stability result for strong detonations to a version of the model featuring diffusion in the z-equation. By assuming a small reaction rate Li, Liu, & Tan [29] were able to obtain a nonlinear stability result for strong detonations. Their technique was based on a combination of spectral analysis and Sattinger's technique [45] of weighted norms. Around the same time, Roquejoffre & Vila [42] examined the spectral stability of strong detonations in the ZND (vanishing viscosity) limit. Their spectral result can be improved to the nonlinear level with the device of weighted norms. Notably, however, outside of the Evans-function framework, we know of *no* stability results for weak-detonation solutions of the Majda model. There are results for weak-detonation solutions of the closely

related Rosales-Majda model

$$u_t + \left(\frac{u^2}{2} - Qz\right)_x = Bu_{xx}\,, \tag{1.2.1a}$$

$$z_x = K\varphi(u)z\,. \tag{1.2.1b}$$

This model was extracted from the physical equations in the Mach $1+\epsilon$ asymptotic regime by Rosales and Majda. Liu & Yu [32] and Szepessy [47] have both treated the stability of weak-detonation solutions of (1.2.1).

1.3 Outline

In Chapter 2 we describe the Majda model and briefly review the existence problem for strong and weak detonations. Because weak detonations are a structurally unstable phenomenon, in this section we also describe our numerical procedure for approximating these waves. In Chapter 3, we set up the spectral stability problem, the construction of the Evans function, and our algorithm for approximating the Evans function and locating its zeros. We also provide an energy estimate that limits possible unstable eigenvalues to a bounded region of the complex plane. The final sections, Chapter 4 and Chapter 5, contain descriptions, results, and interpretations of our various numerical experiments.

Chapter 2. Preliminaries

2.1 Model

2.1.1 Basic Assumptions. We begin with the Majda model [35]:

$$u_t + f(u)_x = Bu_{xx} + qk\varphi(u)z\,, \tag{2.1.1a}$$

$$z_t = Dz_{xx} - k\varphi(u)z\,. \tag{2.1.1b}$$

Here, the scalar unknown u combines various aspects of density, velocity, and temperature. The unknown $z \in [0,1]$ is the mass fraction of reactant. The reaction constants are the heat release $q > 0$ and the reaction rate $k > 0$. As usual, $q > 0$ indicates an exothermic reaction. The diffusion coefficients B and D are also assumed to be positive constants. We make the standard assumption, following [38], that $f \in C^2$ with

$$\frac{\mathrm{d}f}{\mathrm{d}u} > 0\,, \quad \frac{\mathrm{d}^2 f}{\mathrm{d}u^2} > 0\,.$$

We shall use the Burgers flux

$$f(u) = \frac{u^2}{2}$$

as the nonlinearity in our numerical calculations below. Finally, we assume that the ignition function φ is given by

$$\varphi(u) = \begin{cases} 0, & \text{if } u \le u_{\mathrm{ig}}\,, \\ \mathrm{e}^{-E_A/(u-u_{\mathrm{ig}})}, & \text{if } u > u_{\mathrm{ig}}\,, \end{cases}$$

where $E_A > 0$ is the activation energy and u_{ig} is a fixed ignition threshold.

2.2 The Profile Existence Problem

2.2.1 Basic Analysis. We seek traveling wave solutions of the form

$$u(x,t) = \bar{u}(x-st), \quad z(x,t) = \bar{z}(x-st), \quad s > 0, \tag{2.2.1}$$

of (2.1.1) which satisfy

$$\lim_{\xi\to+\infty}(\bar{u}(\xi),\bar{z}(\xi)) = (u_+,z_+) = (u_+,1) \text{ and } \lim_{\xi\to-\infty}(\bar{u}(\xi),\bar{z}(\xi)) = (u_-,z_-) = (u_-,0)\,.$$

These waves move from left to right and leave completely burned gas in their wake. Thus, after dropping the bars, we see that the ansatz (2.2.1) leads from (2.1.1) to the system of ordinary differential equations,

$$-su' + f(u)' = Bu'' + qk\varphi(u)z\,, \tag{2.2.2a}$$

$$-sz' = Dz'' - k\varphi(u)z\,. \tag{2.2.2b}$$

where $'$ denotes differentiation with respect to the variable $\xi := x - st$. After a simple algebraic rearrangement, we can integrate (2.2.2a), and we obtain, finally, the first-order system

$$u' = B^{-1}\big(f(u) - f(u_-) - s(u-u_-) - q(sz+Dy)\big)\,, \tag{2.2.3a}$$

$$z' = y\,, \tag{2.2.3b}$$

$$y' = D^{-1}\big(-sy + k\varphi(u)z\big)\,. \tag{2.2.3c}$$

In (2.2.3), we have written $y := z'$ to express the system in first order. We sometimes write this system compactly as $U' = F(U)$ with $U = (u,z,y)^T$, and we write $A(U) = \mathrm{d}F(U)$. We

require that $u_\pm$ satisfy

$$u_{\rm ig} < u_- \quad \text{and } u_+ < u_{\rm ig} \tag{2.2.4}$$

so that

$$\varphi(u_-) > 0, \quad \varphi(u_+) = 0, \quad \varphi'(u_+) = 0\,. \tag{2.2.5}$$

Equation (2.2.4) is needed so that the unburned state $(u_+, 1)$ is an equilibrium for the traveling-wave equation. Indeed, to guarantee that both $u_\pm$ are equilibria, we require the Rankine-Hugoniot condition

$$f(u_+) - f(u_-) = sq + s(u_+ - u_-)\,, \tag{RH}$$

together with the requirements that $y_\pm = 0$ and $k\varphi(u_\pm)z_\pm = 0$. We write $a_\pm := f'(u_\pm)$. If $u_+ < u_-$, the combustion wave is a *detonation*, and detonations are classified as of *strong*, *weak*, or *Chapman-Jouguet* type according to the relationship between $a_\pm$ and the wave speed s; see Table 2.1. In this paper, we focus on weak detonations.

Strong	$a_- > s > a_+$
Weak	$s > a_-, a_+$
Chapman-Jouguet	$a_- = s > a_+$

Table 2.1: Classification of detonation waves.

The first step in constructing detonation waves is to identify all the possible equilibria of (2.2.3). This amounts to solving (RH). The structure of solutions is well known.

Proposition 2.1 ([38, 35])**.** *Fix u_+. Then, there are 0, 1, or 2 solutions of* (RH) *depending on the wave speed s. In particular, there is a speed $s^{\rm cj}$ depending on u_+ such that*

0. for $s < s^{\rm cj}$, there exist no solutions $u_- > u_+$.,

1. for $s = s^{\rm cj}$ there exists one solution $u_-^{\rm cj}$ (Chapman–Jouguet detonation), and

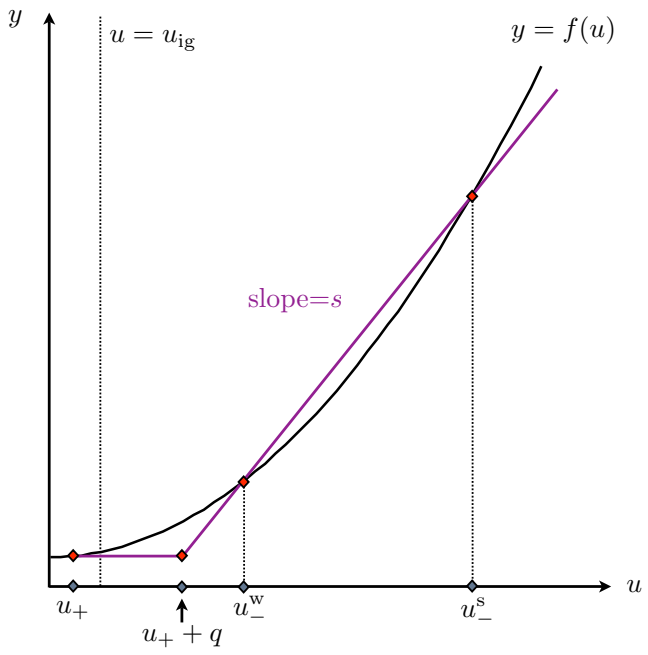

Figure 2.1: The CJ diagram.

2. *for* $s > s^{\mathrm{cj}}$ *there exist two states* $u_-^{\mathrm{s}} > u_-^{\mathrm{w}} > u_+$ *for which* (RH) *(but not necessarily* (2.2.5)*) is satisfied (weak and strong detonation),*

See FIGURE *2.1.*

The case of our principal interest is that the wave is a weak detonation. That is,

$$s > a_+, a_- \,. \tag{2.2.6}$$

We assume, then, that (2.2.6) holds. Linearizing (2.2.3) around the state $(u_-, z_-, y_-) = (u_-, 0, 0)$, we find the system of ordinary differential equations

$$\begin{bmatrix} \hat{u} \\ \hat{z} \\ \hat{y} \end{bmatrix}' = \begin{bmatrix} B^{-1}(a_- - s) & B^{-1}(-sq) & qB^{-1}D \\ 0 & 0 & 1 \\ 0 & kD^{-1}\varphi(u_-) & -sD^{-1} \end{bmatrix} \begin{bmatrix} \hat{u} \\ \hat{z} \\ \hat{y} \end{bmatrix}$$

The coefficient matrix is upper block-triangular, hence one easily sees that it has one positive eigenvalue and two negative eigenvalues. Thus, there is a one-dimensional unstable manifold at $(u_-, 0, 0)$. Similarly, we compute that

$$\begin{bmatrix} \hat{u} \\ \hat{z} \\ \hat{y} \end{bmatrix}' = \begin{bmatrix} B^{-1}(a_+ - s) & B^{-1}(-sq) & qB^{-1}D \\ 0 & 0 & 1 \\ 0 & 0 & -sD^{-1} \end{bmatrix} \begin{bmatrix} \hat{u} \\ \hat{z} \\ \hat{y} \end{bmatrix}.$$

Again using the structure of the coefficient matrix, we see immediately that there are two negative eigenvalues and one zero eigenvalue. It is straightforward to see in this case that the center manifold is a line of equilibria, so no orbit may approach the rest point $(u_+, 1, 0)$ along the center manifold. This follows from the nature of the ignition function φ. Since no trajectory can approach the unburned state along the center manifold, a connection corresponding to a weak detonation corresponds to the intersection of the one-dimensional unstable manifold exiting the burned end state with the two-dimensional stable manifold entering the unburned state in the phase space $\mathbb{R}^3$.

Remark (Strong Detonations). Repeating the above calculation in the case that $a_- > s > a_+$, we see immediately that a strong-detonation connection corresponds to the structurally stable intersection of a pair of two-dimensional manifolds in $\mathbb{R}^3$. See [22] for the examination of the Evans condition $(\star)$ in the case of strong detonations.

The next lemma is immediate by the bounds of the stable (unstable) manifold theorem.

Lemma 2.2 ([35]). *Traveling-wave profiles $(\hat{u}, \hat{z})$ corresponding to weak or strong detonations satisfy*

$$\left| (\mathrm{d}/\mathrm{d}x)^k \Big((\hat{u}, \hat{z})(\xi) - (u, z)_\pm \Big) \right| \leq Ce^{-\theta|\xi|}, \qquad \xi \gtrless 0, \quad 0 \leq k \leq 3\,.$$

2.2.2 End states and parametrization. Suppose $\big(\bar{u}(\xi), \bar{z}(\xi)\big)$ is a traveling-wave profile of (2.1.1a)–(2.1.1b) satisfying (2.2.6). Evidently, $(\bar{u}, \bar{z})$ is a steady solution of

$$u_t - su_x + (u^2/2)_x = Bu_{xx} + qk\varphi(u)z\,, \tag{2.2.7a}$$

$$z_t - sz_x = Dz_{xx} - k\varphi(u)z\,. \tag{2.2.7b}$$

As a preliminary step, we rescale space and time via

$$\tilde{x} = \frac{s}{B}x\,, \quad \tilde{t} = \frac{s^2}{B}t\,;$$

we also rescale u so that

$$s\tilde{u}(\tilde{x}, \tilde{t}) = u(x,t) \quad \text{and} \quad \tilde{z}(\tilde{x}, \tilde{t}) = z(x,t)\,.$$

In the new scaling (2.2.7) takes the form

$$\tilde{u}_{\tilde{t}} - \tilde{u}_{\tilde{x}} + \big(\tilde{u}^2/2\big)_{\tilde{x}} = \tilde{u}_{\tilde{x}\tilde{x}} + \tilde{q}\tilde{k}\tilde{\varphi}(\tilde{u})\tilde{z}$$

$$\tilde{z}_{\tilde{t}} - \tilde{z}_{\tilde{x}} = \tilde{D}\tilde{z}_{\tilde{x}\tilde{x}} - \tilde{k}\tilde{\varphi}(\tilde{u})\tilde{z},$$

where $\tilde{k} = kB/s^2$, $\tilde{\varphi}(\tilde{u}) = \varphi\,(\tilde{u}/s)$, $\tilde{q} = q/s$, and $\tilde{D} = D/B$. We omit the tildes from this point forward giving the system

$$u_t - u_x + \big(u^2/2\big)_x = u_{xx} + qk\varphi(u)z \tag{2.2.9a}$$

$$z_t - z_x = Dz_{xx} - k\varphi(u)z. \tag{2.2.9b}$$

This shows we can take $s = 1$ and the viscosity coefficient $B = 1$. In this case, (RH) reduces to

$$\frac{1}{2}(u_+^2 - u_-^2) = u_+ - u_- + q = 0$$

Consequently we can solve for the burned state u_- in terms of q and u_+

$$u_- = 1 - \sqrt{1 - 2(q + u_+(1 - u_+/2))}. \tag{2.2.10}$$

Therefore, the physical range for q, u_+ is

$$\mathcal{U} := \{(u_+, q) \in \mathbb{R}^2 \,|\, 0 \le u_+ \le u_-, 0 \le q \le \frac{1}{2}(u_+ - 1)^2\}. \tag{2.2.11}$$

2.2.3 Profile Properties. It is worth noting that for $u < u_{ig}$, we can solve the system (2.2.3) explicitly by a simple integration since $\varphi(u) = 0$ for $u < u_{ig}$. In this case we find

$$\begin{aligned} u &= 1 + \beta \tanh(-\beta\xi + C) \\ z &= 1 - CDe^{-\xi/D} \\ y &= Ce^{-\xi/D} \end{aligned}$$

where $\beta = \sqrt{u_-^2 - 2u_- + 2q + 1}$ and C is a constant of integration. We see that u is monotone for $u < u_{ig}$. This is true more generally for weak detonations.

In Majda's original paper he proved that weak detonation solutions of the Majda model have monotonic profiles in the case that $D = 0$ [38]. Majda's proof is given by examining the phase space which, in the $D = 0$ case, is two-dimensional. In the more general case considered here, phase space is three-dimensional adding significantly to the difficulty of the analysis. Here we prove monotonicity in the viscous case by a straightforward examination of the structure of (2.2.3).

Proposition 2.3 (Monotonicity of u)**.** *For any weak detonation profile, u is decreasing in the wave variable ξ.*

Proof. For convenience, define

$$\Phi(u) := \frac{1}{2}(u^2 - u_-) - (u - u_-) = (u - u_-)(\frac{1}{2}(u + u_-) - 1)$$

so that (2.2.3a) can be written

$$u' = \Phi(u) - q(z + Dy).$$

First we claim that for weak detonations $u(\xi) \leq u_-$ for all ξ. Suppose not. Then since $u_- < 1$ for weak detonations, there exists a ξ such that $u_- < u(\xi) < 1$. In this case we see that $\varphi(u(\xi)) < 0$. Notice also that

$$(z + Dy)' = k\varphi(u)z \geq 0.$$

Thus $q(z(\xi) + Dy(\xi)) \geq 0$. Combining these facts implies

$$u'(\xi) = \Phi(u(\xi)) - q(z(\xi) + Dy(\xi)) < 0,$$

a contradiction.

Consequently, there exists some L such that $u'(\xi) < 0$ for all $\xi \leq L$. If u is increasing for some $\xi > L$, then there exists $\xi_1 < \xi_2$ such that $u(\xi_1) = u(\xi_2) = u^*$ (see Figure 2.2). However, $u'(\xi_1) < 0$. So

$$\Phi(u^*) < q(z + Dy)(\xi_1).$$

Since $z + Dy$ is nondecreasing in ξ this implies $\Phi(u^*) < q(z + Dy)(\xi_2)$. Therefore $u'(\xi_2) < 0$,

a contradiction. The desired result follows. □

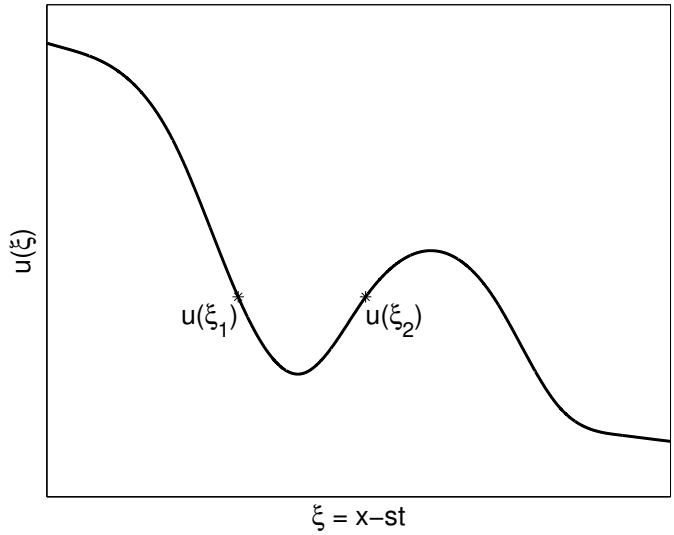

Figure 2.2: Contradictory example considered in the proof monotonicity.

Remark. It is worth noting the implications of the proof for strong detonations. Strong detonation profiles are not all monotone. The proof here fails for strong detonations because for strong detonations $u_- > 1$. Consequently the first claim in the proposition does not hold. The proof does show that for strong detonations a profile cannot move from decreasing to increasing moving left to right. Thus all non-monotonic strong detonation profiles are of the form $u'(\xi) \geq 0$ for $\xi \leq L$ for some L, and $u'(\xi) \leq 0$ for all $\xi \geq L$.

In order for a solution to be physical, we must have that z is nondecreasing since it represents the fraction by mass of reactant. It is worth noting that all solutions satisfy this property.

Proposition 2.4 (Monotonicity of z)**.** *For any profile, z is increasing in the wave variable ξ.*

Proof. Any orbit connecting u_- and u_+ leaves u_- along the unstable manifold into the physical $z > 0$ region. If at any point ξ^* we have $z(\xi^*) > 0$, $z'(\xi^*) = y(\xi^*) = 0$, then

$y' = D^{-1}k\varphi(u)z \geq 0$. Thus $z'' \geq 0$. Consequently, z' is nondecreasing in some neighborhood of ξ^*. Given the explicit form for the portion of a solution with $u < u_{ig}$, this shows that z is monotone increasing. □

2.3 Numerical Approximation of Profiles

2.3.1 Existence. In the case that (2.2.6) holds, we have seen that the existence of a weak detonation requires that the intersection of the two-dimensional stable manifold $W^s(U_+^{\mathrm{w}})$ and the one-dimensional unstable manifold $W^u(U_-)$ form a heteroclinic orbit γ in $\mathbb{R}^3$. Dimension considerations show that this is a structurally unstable intersection. Intuitively, structural instability means that small perturbations can lead to topological changes in the phase portrait. Consequently, we expect that this intersection will only occur for distinguished values of the parameters. Thus, our numerical method for approximating the profile (a necessary step towards the computation of the Evans function) must incorporate a method for determining these parameters.

Beyn describes a method for dealing with this issue of structural instability in [5]. Essentially, we stabilize the system by introducing the parameter k into it as an unknown satisfying the equation $k' = 0$. This will increase the dimension of both the stable and unstable manifolds. Consequently after inflating the state space with the parameter k, we now seek solutions that are the structurally stable intersection of the three dimensional stable manifold at positive infinity and the two-dimensional unstable manifold and negative infinity in $\mathbb{R}^4$.

In doing so we lose control over the value of k when finding solutions. For given values of the other parameters, the solver will return a value of k, if a solution can be found.

2.3.2 Numerical Implementation. In order to obtain numerical solutions, we use projective boundary conditions at $\pm M$ which are given by $\Pi_{\pm}(U(\pm M) - U_{\pm}) = 0$, where $\Pi_{\pm}$ is the matrix whose columns are orthonormal vectors spanning $W^s(U_-^{\mathrm{w}})^{\perp}$ and $W^u(U_+)^{\perp}$ respectively. Because the translation of any solution gives another solution, we also employ a phase boundary condition $u(0) = \frac{1}{2}(u_+ - u_-)$.

The result is a three point boundary value problem. Because most numerical packages are not built to solve a three-point problem, we transform the problem to a two point boundary value problem by doubling the dimension of the problem and halving the domain (see 2.3). Thus we move from the system

$$\begin{bmatrix} u' \\ z' \\ y' \\ k' \end{bmatrix} = U' = f(U), \quad x \in [-M, M]$$

to the system

$$\begin{bmatrix} U' \\ V' \end{bmatrix} = \begin{bmatrix} f(U) \\ -f(V) \end{bmatrix}, \quad x \in [0, M]$$

where in the new system we include three matching boundary conditions of the form $U(0) = V(0)$. We now have a two point boundary value problem which we solve using the MATLAB package bvp6c, a sixth order collocation method utilized by the Evans function package StabLab. (See [4]).

Altogether we have 1 phase condition, 3 projective conditions, and 4 matching conditions which matches the 8 variables in the transformed system. In order to compute numerical solution profiles, the solver will still require a reasonably close initial guess. We find that a rudimentary guess will suffice for intermediate parameter values. For example a guess of the

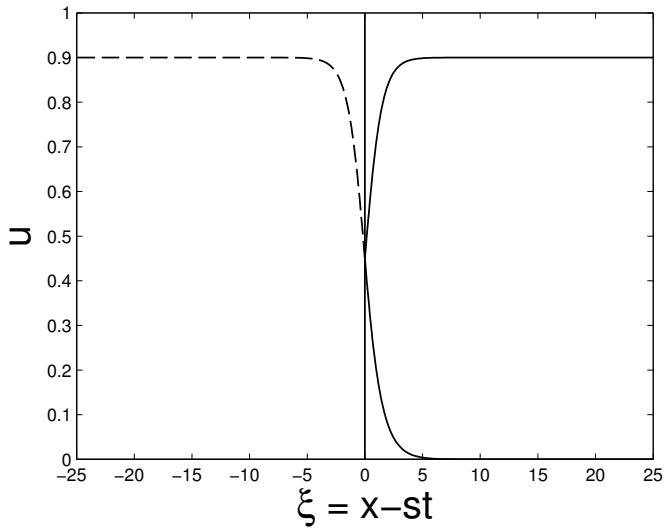

Figure 2.3: We obtain two solutions (the solid lines) on the half domain $[0, M]$. The top curve is reflected across the y-axis which when combined with the bottom curve gives the solution to the original problem.

form

$$u = a - c\tanh(\alpha x) \tag{2.3.1a}$$

$$z = a + c\tanh(\alpha x) \tag{2.3.1b}$$

$$y = \alpha \mathrm{sech}^2(\alpha x) \tag{2.3.1c}$$

for $x \in [0, M]$ where the constants a, c, α are chosen to satisfy the appropriate boundary conditions works well. However, in many parameter regions this is insufficient.

We rely on continuation in regions for which a simple guess is not close enough for the solver to find a solution. That is, we begin in an intermediate parameter region and use the solution for a set of parameters as the initial guess for new parameter values. In this manner we use successive solutions to move to more extreme parameter values. For example a simple guess of the form (2.3.1) may be sufficient to find a solution for parameter values

$q = 0.499$, $D = 1$, $\mathcal{E}_A = 1$. To find a solution profile where we change the parameter q to the value 0.25 (holding $D = \mathcal{E}_A = 1$ fixed), we would use our solution for $q = 0.499$ as an initial guess to find the solution for $q = 0.45$. We would then use that solution as an initial guess to find the solution for $q = 0.40$ and so on until we obtain the desired solution for $q = 0.25$. In some regions of parameter space small changes in parameters can cause larger changes in the shape of solution profiles. In this case the size of the continuation step (that is, the amount we change the parameter value at each step) must be adjusted to be smaller.

2.3.3 Numerical Profile Results. Even with the use of continuation there are many parameter regions for which we are unable to obtain solutions or for which solutions do not exist. In particular we computed solution profiles for values

$$(D, E, q) \in [10^{-3}, 15] \times [10^{-3}, 6] \times [.25, .499].$$

We also tested values varying values of u_+ and u_{ig} but found no qualitative difference and consequently fixed $u_+ = 0$, $u_{ig} = 0.1$. The solutions we were unable to compute in the corners of this parameter space often correspond to extreme, large values of k determined by the solver.

In FIGURE 2.4 we display some examples of the numerically computed solutions of 2.2.3. We note in particular that small values of $\mathcal{E}_A$ result in a large left tail as seen in FIGURE 2.4(d), while large values of D result in a long right tail as seen in FIGURE 2.4(e). In these cases we used continuation and expanded the computational domain in order for the solutions to be within the prescribed tolerance (10^{-3}) of the correct limiting values.

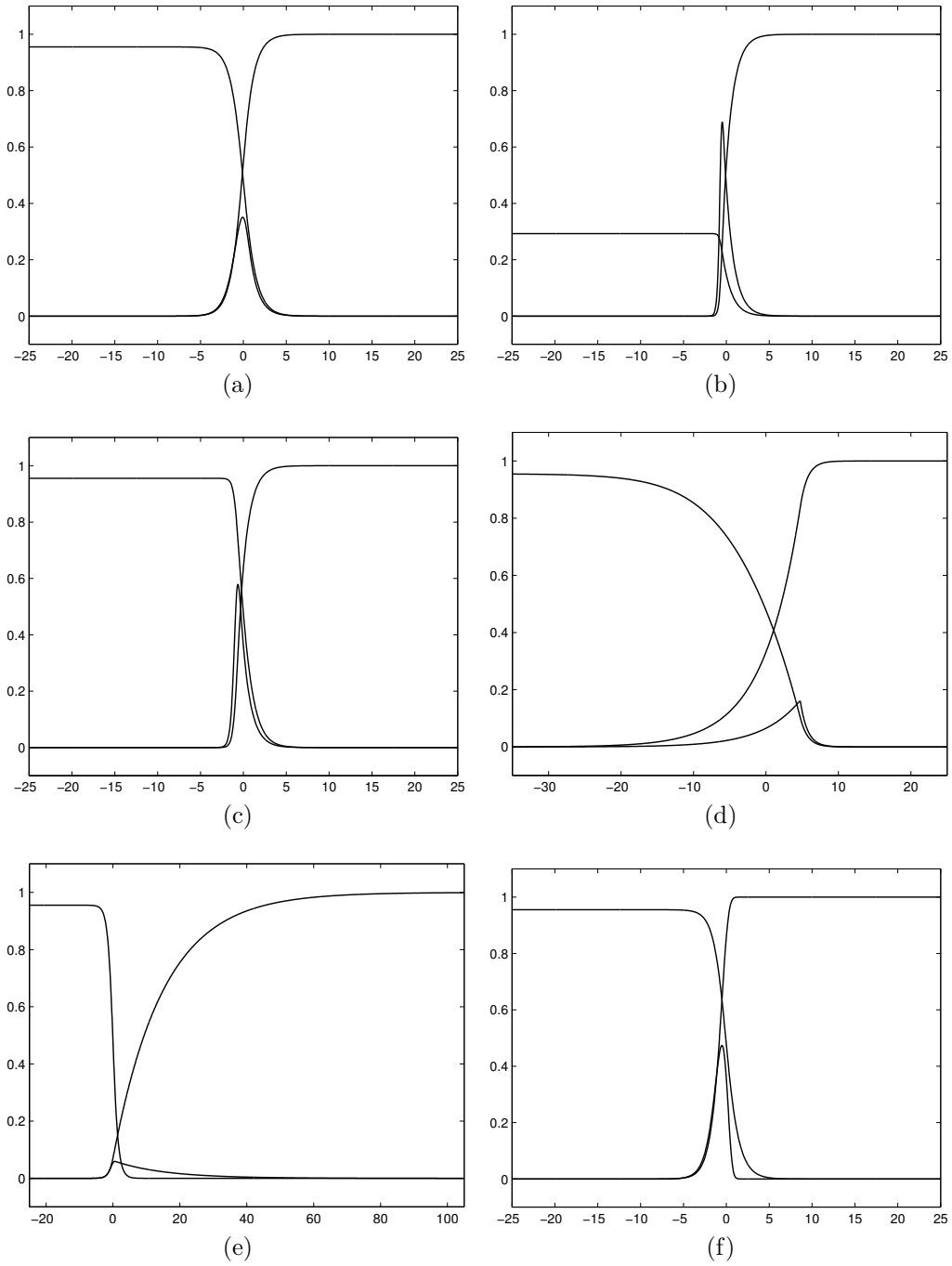

Figure 2.4: Weak detonation profiles for different parameter values. First we consider the intermediate parameter regime ($D = 1$, $\mathcal{E}_A = 1$) for (a) large $q = 0.499$ and (b) small $q = 0.250$. For large q, we also consider (c) large $\mathcal{E}_A$ ($D = 1$, $\mathcal{E}_A = 6$, and $q = 0.499$), (d) small $\mathcal{E}_\mathcal{A}$ ($D = 1$, $\mathcal{E}_A = 10^{-3}$, and $q = 0.499$), (e) large D ($D = 15$, $\mathcal{E}_A = 1$, and $q = 0.499$), and (f) small D ($D = 10^{-3}$, $\mathcal{E}_A = 1$, and $q = 0.499$). Profiles for u, y, and z can be distinguished by noting that $u_- > 0$, $y_- = y_+ = 0$, and $z_+ > 0$.

Chapter 3. Spectral stability

3.1 Linearized equations & eigenvalue problem

To construct the Evans function, we begin by examining the linearization of (2.2.9) about the steady solution $(\hat{u}, \hat{z})$. The linearization can be determined as follows.

Suppose ϵu is a perturbation of $\hat{u}$ and ϵz is a perturbation of $\hat{z}$. Then plugging $\hat{u} + \epsilon u$ and $\hat{z} + \epsilon z$ into (2.2.9) for u and z respectively we have

$$(\hat{u} + \epsilon u)_t - (\hat{u} + \epsilon u)_x + \frac{1}{2}(\hat{u} + \epsilon u)_x^2 = (\hat{u} + \epsilon u)_{xx} + qk(\varphi(\hat{u}) + \varphi'(\hat{u})\epsilon u)(\hat{z} + \epsilon z)$$

noting that $\varphi(u) \approx \varphi(\hat{u}) + \varphi'(\hat{u})\epsilon u$ is the linearization of φ around $\hat{u}$. To get the linearization we keep only the $O(\epsilon)$ terms leaving

$$[\hat{u}_t - \hat{u}_x + \frac{1}{2}(\hat{u})_x^2] + [\epsilon u_t - \epsilon u_x + \epsilon(\hat{u}u)_x] = [\hat{u}_x x + qk\varphi(\hat{u})\hat{z}] + [\epsilon u_x x + qk\epsilon\varphi(\hat{u})z + \epsilon qk\varphi'(\hat{u})u\hat{z}]$$

Noting that $\hat{u}$ and $\hat{z}$ satisfy (2.2.9a), we see that the first bracketed expression on both sides are equal. Thus after dividing out by epsilon we are left with

$$u_t - u_x + (\hat{u}u)_x = u_{xx} + qk\varphi(\hat{u})z + qk\varphi'(\hat{u})u\hat{z}.$$

After rearranging and going through the same process for (2.2.9b) we find that the linearization is

$$\begin{aligned} u_t - q(k\varphi'(\hat{u})u\hat{z} + k\varphi(\hat{u})z) + ((\hat{u} - 1)u)_x &= u_{xx}, \\ z_t - z_x &= -k\varphi'(\hat{u})u\hat{z} - k\varphi(\hat{u})z + Dz_{xx}, \end{aligned}$$

where u, z now denote perturbations.

In order to construct the Evan's function we need to determine the corresponding eigenvalue equations. These can be determined by rewriting the linearization equations in the form

$$u_t = q(k\varphi'(\hat{u})u\hat{z} + k\varphi(\hat{u})z) + ((\hat{u}-1)u)_x + u_{xx}$$
$$z_t = z_x - k\varphi'(\hat{u})u\hat{z} - k\varphi(\hat{u})z + Dz_{xx}.$$

Thus we have two linear operators $u_t = L_u(u)$ and $v_t = L_v(v)$. Then the eigenvalue equations are given by replacing u_t and v_t with λu and λz respectively. Thus corresponding eigenvalue equations are

$$u'' = \lambda u - q(k\varphi'(\hat{u})u\hat{z} + k\varphi(\hat{u})z) + ((\hat{u}-1)u)', \tag{3.1.2a}$$
$$z'' = D^{-1}\big(\lambda z - z' + k\varphi'(\hat{u})u\hat{z} + k\varphi(\hat{u})z\big). \tag{3.1.2b}$$

In (3.1.2) and hereafter $' = \mathrm{d}/\mathrm{d}x$. Alternatively, upon substituting $Dz''-\lambda z+z' = k\varphi'(\hat{u})u\hat{z}+k\varphi(\hat{u})z$ from (3.1.2b) into (3.1.2a), we can rewrite (3.1.2a) as

$$u'' = \lambda(u+qz) - qz' - qDz'' + ((\hat{u}-1)u)'\,. \tag{3.1.3}$$

To construct the Evans function, we write (3.1.2a)–(3.1.2b) as a first-order system. To do so, we define $W := (u, z, u', z')^{\mathrm{t}}$, and we see that the eigenvalue equation can be written as a linear system

$$W' = \mathbb{A}(x;\lambda)W\,,$$

where

$$\mathbb{A}(x;\lambda) = \begin{bmatrix} 0 & 0 & 1 & 0 \\ 0 & 0 & 0 & 1 \\ \lambda + \bar{u}_x - qk\varphi'(\bar{u})\hat{z} & -qk\varphi(\bar{u}) & \bar{u} - 1 & 0 \\ D^{-1}k\varphi'(\bar{u})\bar{z} & D^{-1}\lambda + D^{-1}k\varphi(\bar{u}) & 0 & -D^{-1} \end{bmatrix}.$$

In the case of strong detonations, working with the integrated equations has the advantage of removing the translational zero eigenvalue. While this is not the case for weak detonations, we find that we obtain tighter energy estimates using integrated coordinates. We define $w' := u + qz$ so that (3.1.3) becomes

$$u'' = \lambda w' - qz' - qDz'' - qDz'' + ((\hat{u} - 1)u)'$$

which can be integrated so that the eigenvalue equation becomes

$$u' = \lambda w - qz - qDz' + (\hat{u} - 1)u \tag{3.1.4a}$$

$$w' = u + qz \tag{3.1.4b}$$

$$z'' = D^{-1}(\lambda z - z' + k\varphi'(\hat{u})u\hat{z} + k\varphi(\hat{u})z). \tag{3.1.4c}$$

In matrix form with $X := (u, w, z, z')^t$, (3.1.4) takes the form

$$X' = \mathbb{B}(x;\lambda)X \tag{3.1.5}$$

where

$$\mathbb{B}(x;\lambda) := \begin{bmatrix} \hat{u} - 1 & \lambda & -q & -qD \\ 1 & 0 & q & 0 \\ 0 & 0 & 0 & 1 \\ D^{-1}k\varphi'(\hat{u})\hat{z} & 0 & D^{-1}(\lambda + k\varphi(\hat{u})) & -D^{-1} \end{bmatrix}.$$

Thus we have written the eigenvalue problem as a linear system of first order ODEs where the coefficient matrix depends on x and the spectral parameter λ. We observe that, due to Lemma 2.2, the coefficient matrix $\mathbb{B}$ decays exponentially fast as $x \to \pm\infty$ to a limiting matrix $\mathbb{B}_{\pm}(\lambda)$. The basic idea of the construction of the Evans function is to look for solutions of (3.1.4) which have the "correct" asymptotic behavior, as described by the limiting system $X' = \mathbb{B}_{\pm}(\lambda)X$. Then, roughly speaking, the Evans function can be thought of as a determinant

$$D(\lambda) = \det(\mathcal{W}^{+}(x,\lambda), \mathcal{W}^{-}(x,\lambda))|_{x=0}$$

where $\mathcal{W}^{\pm}$ are bases for the subspaces of solutions of (3.1.5) that decay at $\pm\infty$. Evidently, a zero of $D(\lambda)$ indicates a linear dependence between these subspaces. Such a linear dependence is equivalent to the existence an eigenfunction. We omit the details of the construction. For more details about the construction of the Evans function for the Majda model, see [35]. For more general background information about the Evans function, see, *e.g.*, the survey article of Sandstede [44] and [1, 40, 18].

3.2 High-frequency bounds

We note that the integrated equations (3.1.4) can be written as

$$\lambda w - (1-\hat{u})w' = q\hat{u}z + q(D-1)z' + w'' \tag{3.2.1a}$$

$$\lambda z + k(\varphi(\hat{u}) - q\varphi'(\hat{u})\hat{z})z = z' + k\varphi'(\hat{u})\hat{z}w' + Dz''. \tag{3.2.1b}$$

We show by an energy estimate that any unstable eigenvalue of the integrated eigenvalue equations lies in a bounded region of the unstable half plane. While energy estimates for this system are given in [22], using monotonicity of weak profiles we obtain a modest improvement.

Proposition 3.1 (High-frequency bounds)**.** *Any eigenvalue λ of* (3.2.1) *(weak detonation) with nonnegative real part satisfies*

$$\operatorname{Re}\lambda + |\operatorname{Im}\lambda| \le \max\left\{3, \frac{1}{4D} + \left(\frac{1}{4} + \frac{1}{2}|D-1|^2\right)kL + kM\right\}$$

where

$$L := \sup_{x\in\mathbb{R}} \varphi'(\hat{u}(x))\hat{z} \quad \textit{and} \quad M := \sup_{x\in\mathbb{R}} \left((1+q)\varphi'(\hat{u})\hat{z} - \varphi(\hat{u})\right). \tag{3.2.2}$$

Proof. We multiply (3.2.1a) by $\bar{w}$ and (3.2.1b) by $\bar{z}$ and integrate. In doing so we integrate $w''\bar{w}$, $z''\bar{z}$ and $z'\bar{w}$ terms by parts

$$\begin{aligned}
\int_{\mathbb{R}} w''\bar{w} &= \int_{\mathbb{R}} w'\bar{w}' = \int_{\mathbb{R}} |w'|^2 \\
\int_{\mathbb{R}} z''\bar{z} &= \int_{\mathbb{R}} z'\bar{z}' = \int_{\mathbb{R}} |z'|^2 \\
\int_{\mathbb{R}} z'\bar{w} &= \int_{\mathbb{R}} z\bar{w}'
\end{aligned}$$

noting that the boundary terms are all zero given our required end states.

Then we have

$$\lambda\int_{\mathbb{R}} |w|^2 + \int_{\mathbb{R}} |w'|^2 - \int_{\mathbb{R}} (1-\hat{u})w'\bar{w} = q\int_{\mathbb{R}} \hat{u}z\bar{w} - q(D-1)\int_{\mathbb{R}} z\bar{w}', \tag{3.2.3a}$$

$$\lambda\int_{\mathbb{R}} |z|^2 + D\int_{\mathbb{R}} |z'|^2 + k\int_{\mathbb{R}} (\varphi(\hat{u}) - q\varphi'(\hat{u})\hat{z})|z|^2 = \int_{\mathbb{R}} z'\bar{z} - k\int_{\mathbb{R}} \varphi'(\hat{u})\hat{z}w'\bar{z}. \tag{3.2.3b}$$

Taking the real part of (3.2.3), we find

$$\operatorname{Re}\lambda\int_{\mathbb{R}}|w|^2+\int_{\mathbb{R}}|w'|^2-\operatorname{Re}\left(\int_{\mathbb{R}}(1-\hat{u})w'\bar{w}\right)=\operatorname{Re}\left(q\int_{\mathbb{R}}\hat{u}z\bar{w}-q(D-1)\int_{\mathbb{R}}z\bar{w}'\right), \tag{3.2.4a}$$

$$\operatorname{Re}\lambda\int_{\mathbb{R}}|z|^2+D\int_{\mathbb{R}}|z'|^2+k\int_{\mathbb{R}}(\varphi(\hat{u})-q\varphi'(\hat{u})\hat{z})|z|^2=-\operatorname{Re}\left(k\int_{\mathbb{R}}\varphi'(\hat{u})\hat{z}w'\bar{z}\right). \tag{3.2.4b}$$

Similarly, taking the imaginary part of (3.2.3), we observe

$$\operatorname{Im}\lambda\int_{\mathbb{R}}|w|^2-\operatorname{Im}\left(\int_{\mathbb{R}}(1-\hat{u})w'\bar{w}\right)=\operatorname{Im}\left(q\int_{\mathbb{R}}\hat{u}z\bar{w}-q(D-1)\int_{\mathbb{R}}z\bar{w}'\right), \tag{3.2.5a}$$

$$\operatorname{Im}\lambda\int_{\mathbb{R}}|z|^2=\operatorname{Im}\left(\int_{\mathbb{R}}z'\bar{z}-k\int_{\mathbb{R}}\varphi'(\hat{u})\hat{z}w'\bar{z}\right)=0. \tag{3.2.5b}$$

Here we make two observations. First

$$\begin{aligned}\int_{\mathbb{R}}w'\bar{w}&=-\int_{\mathbb{R}}w\bar{w}'\\&=-\overline{\int_{\mathbb{R}}\bar{w}w'}\end{aligned}$$

where the first equality comes from integration by parts. Thus $\int_{\mathbb{R}}w'\bar{w}$ is imaginary.

Second,

$$\int_{\mathbb{R}}\hat{u}w'\bar{w}=-\int_{\mathbb{R}}(\hat{u}\bar{w})'w \tag{3.2.6}$$

$$=-\int_{\mathbb{R}}(\hat{u}'\bar{w}+\hat{u}\bar{w}')w \tag{3.2.7}$$

$$=-\int_{\mathbb{R}}\hat{u}'|w|^2-\int_{\mathbb{R}}\hat{u}\bar{w}'w \tag{3.2.8}$$

$$=-\int_{\mathbb{R}}\hat{u}'|w|^2-\overline{\int_{\mathbb{R}}\hat{u}w'\bar{w}} \tag{3.2.9}$$

Therefore we have

$$\operatorname{Re}\left(\int_{\mathbb{R}} \hat{u} w' \bar{w}\right) = -\frac{1}{2}\int_{\mathbb{R}} \hat{u}'|w|^2 > 0$$

since by Proposition 2.3 $u' < 0$.

Putting these facts together we have

$$\operatorname{Re}\left(\int_{\mathbb{R}} (1-\hat{u}) w' \bar{w}\right) = \frac{1}{2}\int_{\mathbb{R}} \hat{u}'|w|^2 < 0. \tag{3.2.10}$$

Using the fact that $\operatorname{Re} x + |\operatorname{Im} x| \leq \sqrt{2}|x|$, we combine (3.2.4) and (3.2.5) to get

$$\begin{aligned}\big(\operatorname{Re}\lambda + |\operatorname{Im}\lambda|\big)\int_{\mathbb{R}} |w|^2 + \int_{\mathbb{R}} |w'|^2 \\ \leq \sqrt{2}q\int_{\mathbb{R}} \hat{u}|z||w| + \sqrt{2}q|D-1|\int_{\mathbb{R}} |z||w'| + \int_{\mathbb{R}} |1-\hat{u}||w'||w|,\end{aligned} \tag{3.2.11}$$

and

$$\begin{aligned}\big(\operatorname{Re}\lambda + |\operatorname{Im}\lambda|\big)\int_{\mathbb{R}} |z|^2 + k\int_{\mathbb{R}} (\varphi(\hat{u}) - q\varphi'(\hat{u})\hat{z})|z|^2 + D\int_{\mathbb{R}} |z'|^2 \\ \leq \int_{\mathbb{R}} |z'||z| + \sqrt{2}k\int_{\mathbb{R}} |\varphi'(\hat{u})\hat{z}||w'||z|\,.\end{aligned} \tag{3.2.12}$$

Note the term $\int_{\mathbb{R}} |1-\hat{u}||w'||w|$ is not multiplied by $\sqrt{2}$ because we can drop the real part because of (3.2.10).

We now recall the general form of Young's inequality:

$$ab \leq \epsilon a^p + \frac{1}{4\epsilon} b^q$$

where $a, b, \epsilon \geq 0$ and $p, q > 0$ with $\frac{1}{p} + \frac{1}{q} = 1$.

Using Young's inequality (several times, with $p = q = 2$) together with the assumption

that $\operatorname{Re}\lambda \geq 0$, we find that inequalities (3.2.11) and (3.2.12) imply

$$\begin{aligned}\big(\operatorname{Re}\lambda + |\operatorname{Im}\lambda|\big)\int_{\mathbb{R}}|w|^2 + \int_{\mathbb{R}}|w'|^2 &\leq \sqrt{2}q\|\hat{u}\|_\infty \int_{\mathbb{R}}\left(\varepsilon_1|z|^2 + \frac{|w|^2}{4\varepsilon_1}\right)\\ &+ \sqrt{2}q|D-1|\int_{\mathbb{R}}\left(\varepsilon_2|z|^2 + \frac{|w'|^2}{4\varepsilon_2}\right) + \|1-\hat{u}\|_\infty \int_{\mathbb{R}}\left(\varepsilon_3|w'|^2 + \frac{|w|^2}{4\varepsilon_3}\right) \quad (3.2.13)\end{aligned}$$

and

$$\begin{aligned}\big(\operatorname{Re}\lambda + |\operatorname{Im}\lambda|\big)\int_{\mathbb{R}}|z|^2 + k\int_{\mathbb{R}}(\varphi(\hat{u}) - q\varphi'(\hat{u})\hat{z})|z|^2 + D\int_{\mathbb{R}}|z'|^2\\ \leq \int_{\mathbb{R}}\left(\varepsilon_4|z'|^2 + \frac{|z|^2}{4\varepsilon_4}\right) + \sqrt{2}kL\int_{\mathbb{R}}\left(\varepsilon_5|w'|^2 + \frac{|z|^2}{4\varepsilon_5}\right). \quad (3.2.14)\end{aligned}$$

We multiply (3.2.14) by $\Theta > 0$ and add the result to (3.2.13). The result is

$$\begin{aligned}\big(\operatorname{Re}\lambda + |\operatorname{Im}\lambda|\big)\left(\int_{\mathbb{R}}|w|^2 + \Theta|z|^2\right) + k\int_{\mathbb{R}}\varphi(x)|z|^2 + \int_{\mathbb{R}}|w'|^2 + \Theta D\int_{\mathbb{R}}|z'|^2\\ \leq \int_{\mathbb{R}}R_1(x)\Theta|z|^2 + \varepsilon_4\Theta\int_{\mathbb{R}}|z'|^2 + R_2\int_{\mathbb{R}}|w'|^2 + R_3\int_{\mathbb{R}}|w|^2 \quad (3.2.15)\end{aligned}$$

where

$$\begin{aligned}\varphi(x) &= (\varphi(\hat{u}) - q\varphi'(\hat{u})\hat{z}),\\ R_1(x) &= \frac{\sqrt{2}\varepsilon_1 q\|\hat{u}\|_\infty}{\Theta} + \frac{\sqrt{2}\varepsilon_2 q|D-1|}{\Theta} + \frac{1}{4\varepsilon_4} + \frac{\sqrt{2}kL}{4\varepsilon_5},\\ R_2 &= \sqrt{2}\left(\frac{q|D-1|}{4\varepsilon_2} + \frac{\varepsilon_3\|1-\hat{u}\|_\infty}{\sqrt{2}} + \varepsilon_5\Theta kL\right),\end{aligned}$$

and

$$R_3 = \sqrt{2}\left(\frac{q\|\hat{u}\|_\infty}{4\varepsilon_1} + \frac{\|1-\hat{u}\|_\infty}{4\sqrt{2}\varepsilon_3}\right).$$

Finally, to simplify (3.2.15), we choose

$$\begin{aligned}
\varepsilon_1 &= \frac{\sqrt{2}}{8} & \varepsilon_2 &= \sqrt{2}q|D-1| \\
\varepsilon_3 &= \frac{2}{8\|1-\hat{u}\|_\infty} & \varepsilon_4 &= D \\
\varepsilon_5 &= \frac{\sqrt{2}}{4} & \Theta &= (kL)^{-1},
\end{aligned}$$

where L and M are as in (3.2.2). We also note that $\|\hat{u}\|_\infty \le 2$, $\|1-\hat{u}\|_\infty \le 1$, and $q \le 1/2$. Thus, we have

$$\begin{aligned}
\big(\operatorname{Re}\lambda + |\operatorname{Im}\lambda|\big)\int_{\mathbb{R}}(|w|^2+\Theta|z|^2) &\le 3\int_{\mathbb{R}}|w|^2 + C\int_{\mathbb{R}}\Theta|z|^2 \\
&\le \max(3,C)\int_{\mathbb{R}}(|w|^2+\Theta|z|^2), \qquad (3.2.16)
\end{aligned}$$

where

$$C := \left(\frac{1}{4D} + \left(\frac{1}{4}+\frac{1}{2}|D-1|^2\right)kL + kM\right).$$

The result follows from dividing both sides of (3.2.16) by $\int_{\mathbb{R}}(|w|^2+\Theta|z|^2)$. □

Remark. We easily obtain the following crude bounds on L and M:

$$\begin{aligned}
L &\le \sup_{x\in\mathbb{R}}\varphi'(\hat{u}(x)) \le \varphi'\left(u_{\text{ig}}+\frac{\mathcal{E}_A}{2}\right) = \frac{4}{\mathcal{E}_A}\varphi\left(u_{\text{ig}}+\frac{\mathcal{E}_A}{2}\right) \le \frac{4}{\mathcal{E}_A}\mathrm{e}^{-2} \approx \frac{0.5413}{\mathcal{E}_A}, \\
M &\le \sup_{x\in\mathbb{R}}(1+q)\varphi'(\hat{u}) \le \frac{6}{\mathcal{E}_A}\mathrm{e}^{-2} \approx \frac{0.8120}{\mathcal{E}_A}.
\end{aligned}$$

3.3 Evans Function

As outlined above, the Evans function $D(\lambda)$ acts as a kind of characteristic polynomial for the linear operator L; that is,

$$D(\lambda_0) = 0 \Leftrightarrow \ \lambda_0 \text{ is an eigenvalue of } L.$$

Unfortunately, it is seldom possible to explicitly compute the Evans function; however, it is possible to approximate it numerically [24]. Since the $D(\lambda)$ is analytic on the unstable half plane, it is possible to seek zeros by winding number computations. The origins of this approach to stability can be found in the work of Evans and Feroe [14]. These ideas have since been used to address the stability of traveling-wave solutions to a number of systems of interest; see, *e.g.*, [39, 2, 8, 7].

Techniques for the numerical approximation of the Evans function have been described in detail elsewhere [8, 23, 24], so we only summarize the important aspects of the computation here.

(i) We approximate the profile on a finite computational domain $[-M_-, M_+]$. The computational values for plus and minus spatial infinity, $M_\pm$, must be chosen with some care. Writing the traveling-wave equation (2.2.3) as $U' = F(U)$ together with the condition that $U \to U_\pm$ as $\xi \to \pm\infty$, the typical requirement is that $M_\pm$ should be chosen so that $|U(\pm M_\pm) - U_\pm|$ is within a prescribed tolerance. We use a tolerance of 10^{-3}.

(ii) For each profile compute the high-frequency spectral bounds given by Proposition 3.1. To do so we must compute L and M from (3.2.2). From the bounds we can determine a positive real number R sufficiently large so that no eigenvalue of (3.1.4) lies outside B_R^+, the half circle of radius R in the positive half-plane $\Re(\lambda) \geq 0$. Now we need only establish that the Evans function has no zeros in the bounded region B_R^+.

(iii) Given the solution profiles and appropriate bound from the previous step, we evaluate the Evans function by use of the StabLab package, a MatLab-based package developed for Evans function computation [4]. We use the polar-coordinate method [24] for the computation and Kato's method [26, p. 99] to analytically determine the initial eigenvectors; details of these methods are described in [9, 7, 23]. Throughout our study, we set the tolerances on MATLAB's stiff ODE solver `ode15s` to be `RelTol = 1e-6` and `AbsTol = 1e-8`.

(iv) We compute the number of zeros of the Evans function inside the contour $S = \partial B_R^+$ by computing the winding number of the image of S under the Evans function. By The Argument Principle, since the Evans function is analytic, the winding number of the image will be equal to the number of zeros inside the preimage contour (see Figure 3.1). This is also computed using the StabLab package by choosing a set of λ-values on S for which we sum the changes in $\arg E(\lambda)$ as we traverse S counterclockwise. We add λ values to our set if the change in $\arg E(\lambda)$ is greater than 0.2 in any step. By Rouché's theorem, we are guaranteed to have an accurate computation of the winding number if the argument varies by less than $\pi/2$ between two λ values [20].

As mentioned previously, the shift to integrated coordinates does not remove the translational zero eigenvalue for weak detonations. In order to use the winding number technique just described, the image contour cannot cross through zero; consequently, we must first remove the zero eigenvalue in another way. In this case we find that since the zero eigenvalue has multiplicity one, we can simply divide the Evans function by λ to remove that zero.

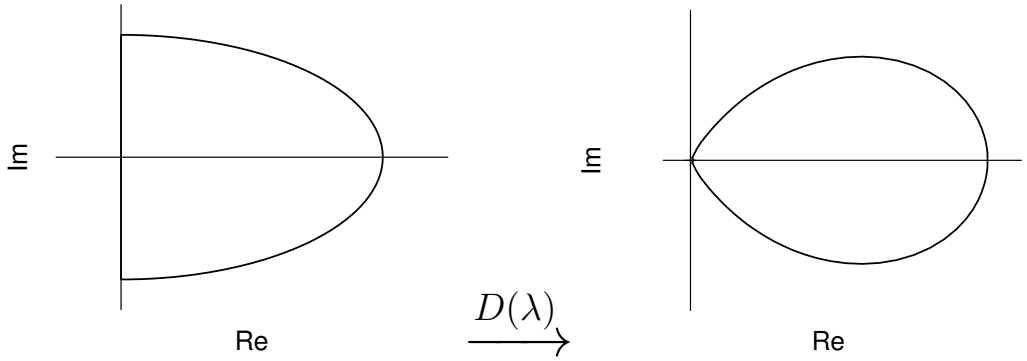

Figure 3.1: We take a closed contour that contains the bounded region of the right half-plane obtained from the high frequency bounds. After mapping by the Evans function we obtain the image contour. If the origin is inside the contour then the winding number is positive, implying the Evans function has a zero in the right half plane. Often, as is the case in this picture, the Evans function comes very near the origin but upon zooming in it can be seen that it does not enclose the origin.

Chapter 4. Experiments

We now discuss our experiments. Recall that $s = 1$, and $u_- \in (u_+, 1)$ is determined by (2.2.10). Also, the parameter k was used in inflating the state space and thus given values for the other parameters, a value of k for which a solution can be found is determined by the boundary value solver. While u_+ can take values specified by (2.2.11), we find no qualitative differences for varied values of u_+ and thus we fix $u_+ = 0$. We also find no qualitative difference in letting u_{ig} vary and so we set $u_{ig} = 0.1$ throughout. These values of u_+ and u_{ig} correspond with those used in [22]. In this case (2.2.10) and (2.2.11), imply $q \in [0, \frac{1}{2})$ in order to ensure $u_- < 1$, the condition for a weak detonation.

We let the parameters q, E, and D vary through the ranges $[0.250, 0.499]$, $[10^{-3}, 6]$, and $[10^{-3}, 15]$ respectively. We find profiles to be stable throughout the parameter region computed. However, we were not able to obtain solutions for all values of the parameters in the specified region. In particular, as we move toward the boundaries of this parameter space we typically find that we must take smaller continuation steps until we hit a point that continuing is no longer feasible.

In this section we consider the specific behavior of the Evans function as we vary the activation energy E and the viscosity constant D across values of q. We find that as we allow q to decrease, the parameter k increases to extreme values. For example, if we fix $D = 1$ and $\mathcal{E}_A = 1$, then for $q = 0.499$, the corresponding value of k is 8.177. However for $q = 0.250$, k increases to approximately $7,913$. In such regions where k begins to blow up we generally cannot continue to find solutions.

4.1 Activation Energy

First we consider activation energy, $\mathcal{E}_A$, allowing it to take values in $[10^{-3}, 6]$. We find that just as k increases with decreasing values of q, it also increases as $\mathcal{E}_A$ increases. For example, if we fix $q = 0.499$ $D = 1$, then for $\mathcal{E}_A = 10^{-3}$ we find $k = 0.236$. However for $\mathcal{E}_A = 6$ we have $k \approx 21,600$.

In Figure 4.1 (a) and (b), we see the Evans function output for large values of $\mathcal{E}_A$. For low values of q we see a single loop in the Evans function. As q increases we see the loop break into two loops which then disappear altogether. We see that the contours do not enclose the origin, demonstrating that the images have winding number zero. Thus the corresponding profiles are stable. We note image contours for smaller values of q maintain a greater distance from the origin suggesting that there is stability, even in the case of q smaller than those for which we were able to compute profiles.

In Figure 4.1 (c) and (d), we see the Evans function output for small values of $\mathcal{E}_A$. The larger image contours correspond to larger values of q. Once again, for smaller values of q we see that the image contours move away from the origin suggesting stability even in the case of q smaller than those computed.

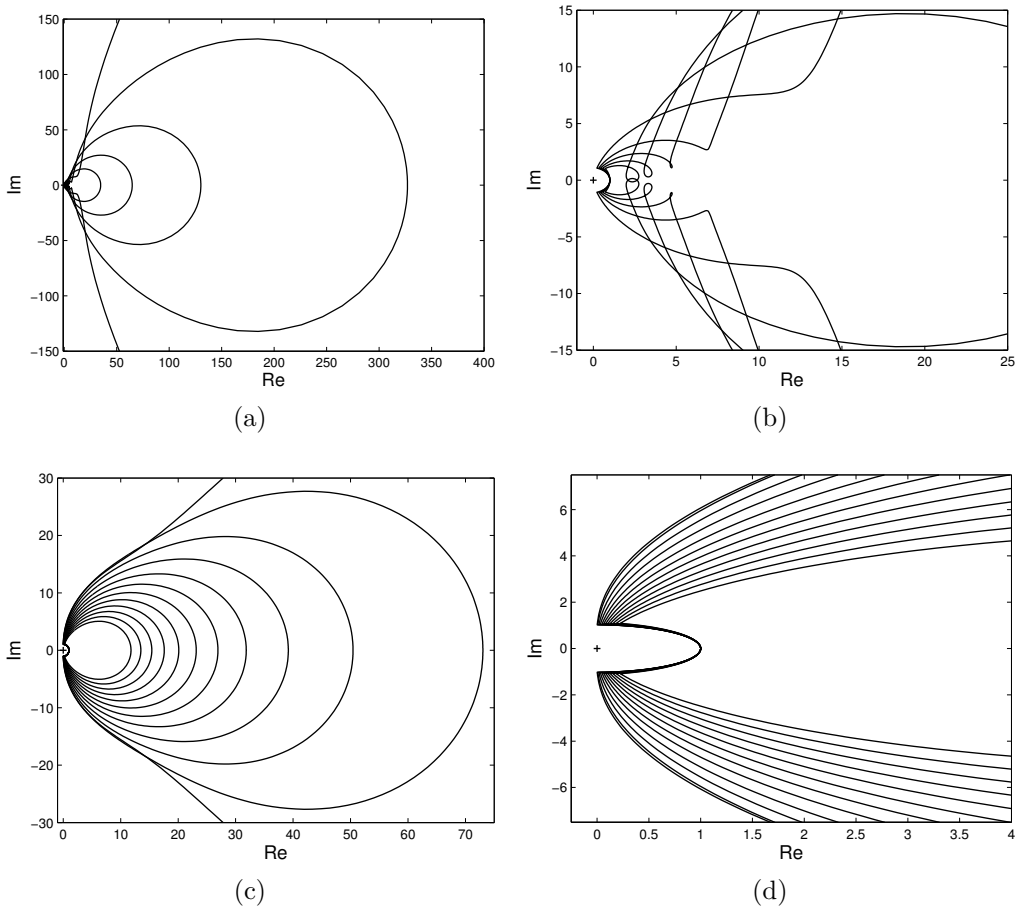

Figure 4.1: Evans function output for extreme values of $\mathcal{E}_A$ with $D = 1$. The parameter values are (a) $\mathcal{E}_A = 3.2$ with q varying through $[.4, .499]$ and (c) $\mathcal{E}_A = 10^{-3}$ with q varying through $[.25, .499]$. Figures (b) and (d) are zoomed in versions of (a) and (c). The origin is marked with a '+'.

4.2 Viscosity

We also consider values of the viscosity constant D in the range $[10^{-3}, 15]$. For changes in D we do not see the extreme changes in K that occur for activation energy. As such we find that we are able to more easily obtain profiles across parameter space.

In Figure 4.2 (a) and (b), we see the Evans function output for large values of D. In this case contours grow larger for smaller q values. For all levels of q the image contours have an intrusion pointing away from the origin that ensures the contours do not contain

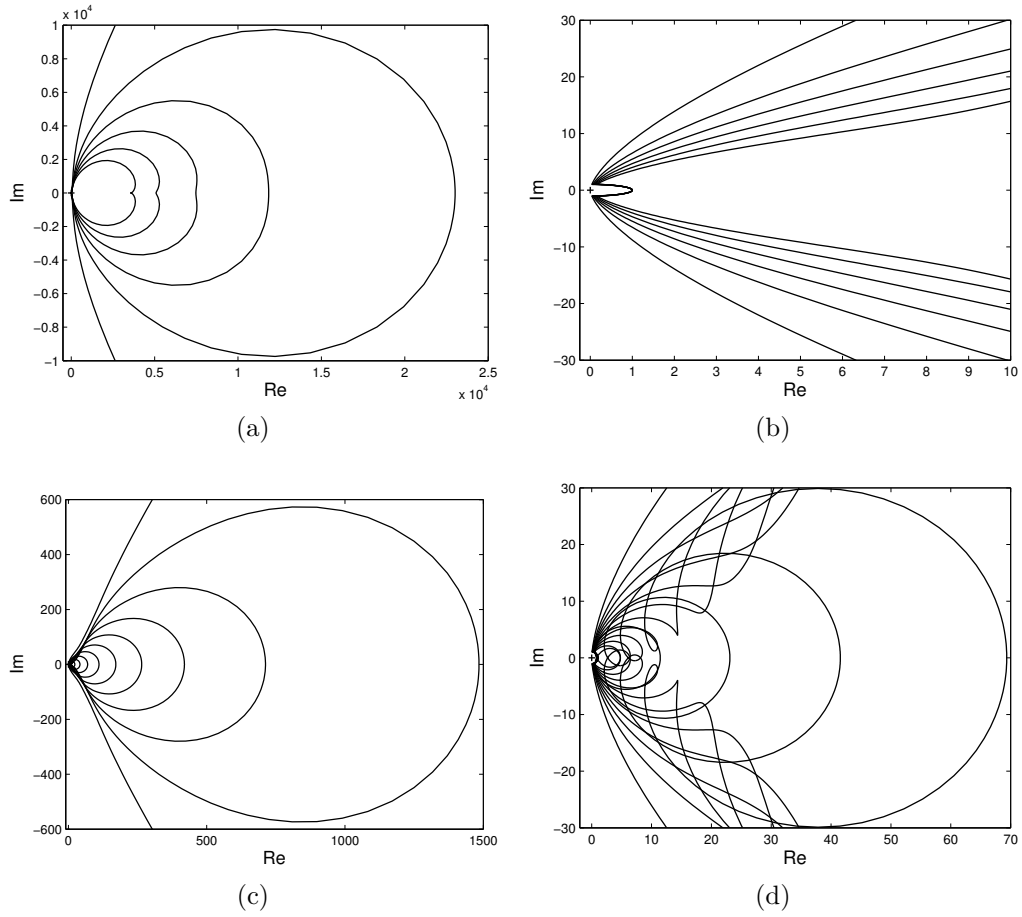

Figure 4.2: Evans function output for extreme values of D with $\mathcal{E}_A = 1$. The parameter values are (a) $D = 15$ with q varying through $[.38, .499]$ and (c) $D = .14$ with q varying through $[.27, .499]$. Figures (b) and (d) are zoomed in versions of (a) and (c). The origin is marked with a '+'.

the origin and that the corresponding profiles are stable.

In FIGURE 4.2 (c) and (d), we see the Evans function output for small values of D. For small values of D we see significant change in the shape of contours as q varies. For larger values of q the image contours are larger, but contain no interesting features. For decreasing values of q, we first see a protrusion pointing toward the origin. As q continues to decrease we see the protrusion form two loops as it connects to the rest of the contour. Near the lowest values of q computed we see these loops begin to overlap almost entirely.

Chapter 5. Conclusions

The main contribution of this thesis is demonstrating via Evans function computation that weak detonation solutions to the Majda model are stable. We have found that solutions are stable throughout the parameter space tested. This improves understanding of the Majda model in itself and also improves the understanding of how Majda's simplified combustion model relates to more complete physical models such as the reactive Navier-Stokes equations.

In the process of computing profiles and evaluating the Evans function we have also demonstrated the use of techniques for solving shockwave boundary value problems. We demonstrated the formulation of appropriate boundary conditions. We showed how to convert a three point boundary value problem into a two point boundary value problem. Most notably, we have used the method of inflating the state space in order to deal with the issue of structural instability.

This paper also gives some analysis of the viscous Majda model. Much of the previous analytical work on Majda's model (particularly for weak detonations) has been done in the much simpler $D = 0$ case. By allowing $D \neq 0$ the difficulty of the analysis and numerics is increased significantly as it adds a dimension to the resulting system of ODEs. In particular we have given a proof of the monotonicity of weak detonation solutions to the viscous Majda model. There is no other existing proof of this fact of which we are aware.

Bibliography

[1] J. Alexander, R. Gardner, and C. Jones. A topological invariant arising in the stability analysis of travelling waves. *J. Reine Angew. Math.*, 410:167–212, 1990.

[2] J. C. Alexander and R. Sachs. Linear instability of solitary waves of a Boussinesq-type equation: a computer assisted computation. *Nonlinear World*, 2(4):471–507, 1995.

[3] Leanne Allen and Thomas J. Bridges. Numerical exterior algebra and the compound matrix method. *Numer. Math.*, 92(2):197–232, 2002.

[4] Blake Barker, Jeffrey Humpherys, and Kevin Zumbrun. Stablab: A matlab-based numerical library for Evans function computation, 2009.

[5] W.-J. Beyn. The numerical computation of connecting orbits in dynamical systems. *IMA J. Numer. Anal.*, 10(3):379–405, 1990.

[6] Anne Bourlioux and Andrew J. Majda. Theoretical and numerical structure of unstable detonations. *Philosophical Transactions: Physical Sciences and Engineering*, 350(1692):29–68, 1995.

[7] Thomas J. Bridges, Gianne Derks, and Georg Gottwald. Stability and instability of solitary waves of the fifth-order kdv equation: a numerical framework. *Phys. D*, 172(1-4):190–216, 2002.

[8] Leon Q. Brin. Numerical testing of the stability of viscous shock waves. *Math. Comp.*, 70(235):1071–1088, 2001.

[9] Leon Q. Brin and Kevin Zumbrun. Analytically varying eigenvectors and the stability of viscous shock waves. *Mat. Contemp.*, 22:19–32, 2002. Seventh Workshop on Partial Differential Equations, Part I (Rio de Janeiro, 2001).

[10] J Buckmaster and J. Neves. One-dimensional detonation stability: the spectrum for infinite activation energy. *Phys. Fluids*, 31:3571–3576, 1988.

[11] Gui-Qiang Chen, David Hoff, and Konstantina Trivisa. Global solutions to a model for exothermically reacting, compressible flows with large discontinuous initial data. *Arch. Ration. Mech. Anal.*, 166(4):321–358, 2003.

[12] Phillip Colella, Andrew Majda, and Victor Roytburd. Theoretical and numerical structure for reacting shock waves. *SIAM J. Sci. Statist. Comput.*, 7(4):1059–1080, 1986.

[13] R. Courant and K. O. Friedrichs. *Supersonic flow and shock waves*. Springer-Verlag, 1976. Reprinting of the 1948 original; Applied Mathematical Sciences, Vol. 21.

[14] J.W. Evans and J. A. Feroe. Traveling waves of infinitely many pulses in nerve equations. *Math. Biosci.*, 37:23–50, 1977.

[15] Wildon Fickett. Detonation in miniature. *Am. J. Phys.*, 47(12):1050–1059, 1979.

[16] Wildon Fickett and William Davis. *Detonation: Theory and Experiment*. Dover, 2000. corrected reprint of 1979 UC Berkeley Edition.

[17] Paul C. Fife. Propagating fronts in reactive media. Nonlinear problems: present and future (Los Alamos, N.M., 1981), North-Holland Math. Stud., vol. 61, North-Holland, Amsterdam, 1982. pp. 267–285.

[18] Kevin Gardner, Robert A.and Zumbrun. The gap lemma and geometric criteria for instability of viscous shock profiles. *Comm. Pure Appl. Math.*, 51(7):797–855, 1998.

[19] Robert A. Gardner. On the detonation of a combustible gas. *Trans. Amer. Math. Soc.*, 277(2):431–468, 1983.

[20] Peter Henrici. *Applied and computational complex analysis. Vol. 1.* Wiley Classics Library. John Wiley & Sons Inc., 1988. Power series—integration—conformal mapping—location of zeros; Reprint of the 1974 original; A Wiley-Interscience Publication.

[21] Jeffrey Humpherys, Gregory Lyng, and Kevin Zumbrun. Spectral stability of ideal-gas shock layers. *Arch. Ration. Mech. Anal.*, 194(3):1029–1079, 2009.

[22] Jeffrey Humpherys, Gregory Lyng, and Kevin Zumbrun. Spectral stability combustion waves: the Majda model. *preprint*, 2012.

[23] Jeffrey Humpherys, Björn Sandstede, and Kevin Zumbrun. Efficient computation of analytic bases in Evans function analysis of large systems. *Numer. Math.*, 103(4):631–642, 2006.

[24] Jeffrey Humpherys and Kevin Zumbrun. An efficient shooting algorithm for Evans function calculations in large systems. *Phys. D*, 220(2):116–126, 2006.

[25] Soyeun Jung and Jinghua Yao. Stability of znd detonations for Majda's model. *Quarterly of Applied Mathematics*. to appear.

[26] Tosio Kato. *Perturbation theory for linear operators*. Classics in Mathematics. Springer-Verlag, 1995. Reprint of the 1980 edition.

[27] Bernard Larrouturou. Remarks on a model for combustion waves. *Nonlinear Anal.*, 9(9):905–935, 1985.

[28] Arnon Levy. On Majda's model for dynamic combustion. *Comm. Partial Differential Equations*, 17(3-4):657–698, 1992.

[29] Dening Li, Tai-Ping Liu, and Dechun Tan. Stability of strong detonation travelling waves to combustion model. *J. Math. Anal. Appl.*, 201(2):516–531, 1996.

[30] Jiequan Li and Peng Zhang. The transition from Zeldovich-von Neumann-Doring to Chapman-Jouguet theories for a nonconvex scalar combustion model. *SIAM J. Math. Anal.*, 34(3):675–699 (electronic), 2002.

[31] Tai-Ping Liu and Long An Ying. Nonlinear stability of strong detonations for a viscous combustion model. *SIAM J. Math. Anal.*, 26(3):519–528, 1995.

[32] Tai-Ping Liu and Shih-Hsien Yu. Nonlinear stability of weak detonation waves for a combustion model. *Comm. Math. Phys.*, 204(3):551–586, 1999.

[33] Tai-Ping Liu and Tong Zhang. A scalar combustion model. *Arch. Rational Mech. Anal.*, 114(4):297–312, 1991.

[34] J. David Logan and Steven R. Dunbar. Travelling waves in model reacting flows with reversible kinetics. *IMA J. Appl. Math.*, 49(2):103–121, 1992.

[35] Gregory Lyng, Mohammadreza Raoofi, Benjamin Texier, and Kevin Zumbrun. Pointwise green function bounds and stability of combustion waves. *J. Differential Equations*, 233(2):654–698, 2007.

[36] Gregory Lyng and Kevin Zumbrun. One-dimensional stability of viscous strong detonation waves. *Arch. Ration. Mech. Anal.*, 173(2):213–277, 2004.

[37] Gregory Lyng and Kevin Zumbrun. A stability index for detonation waves in Majda's model for reacting flow. *Phys. D*, 194(1-2):1–29, 2004.

[38] Andrew Majda. A qualitative model for dynamic combustion. *SIAM J. Appl. Math.*, 41(1):70–93, 1981.

[39] Robert L. Pego, Peter Smereka, and Michael I. Weinstein. Oscillatory instability of traveling waves for a KdV-Burgers equation. *Phys. D*, 67(1-3):45–65, 1993.

[40] Robert L. Pego and Michael I. Weinstein. Eigenvalues, and instabilities of solitary waves. *Philos. Trans. Roy. Soc. London Ser. A*, 340(1656):47–94, 1992.

[41] Abdolrahman Razani. Existence of Chapman-Jouguet detonation for a viscous combustion model. *J. Math. Anal. Appl.*, 293(2):551–563, 2004.

[42] Jean-Michel Roquejoffre and Jean-Paul Vila. Stability of ZND detonation waves in the Majda combustion model. *Asymptot. Anal.*, 18(3-4):329–348, 1998.

[43] Rodolfo R. Rosales and Andrew Majda. Weakly nonlinear detonation waves. *SIAM J. Appl. Math.*, 43(5):1086–1118, 1983.

[44] Björn Sandstede. Stability of travelling waves. *Handbook of dynamical systems, Vol. 2*, pages 983–1055, North-Holland, Amsterdam, 2002.

[45] D. H. Sattinger. On the stability of waves of nonlinear parabolic systems. *Advances in Math.*, 22(3):312–355, 1976.

[46] Wan Cheng Sheng and De Chun Tan. Weak deflagration solutions to the simplest combustion model. *J. Differential Equations*, 107(2):207–230, 1994.

[47] Anders Szepessy. Dynamics and stability of a weak detonation wave. *Comm. Math. Phys.*, 202(3):547–569, 1999.

[48] Benjamin Texier and Kevin Zumbrun. Relative Poincaré-Hopf bifurcation and galloping instability of traveling waves. *Methods Appl. Anal.*, 12(4):349–380, 2005.

[49] Benjamin Texier and Kevin Zumbrun. Galloping instability of viscous shock waves. *Phys. D*, 237(10-12):1553–1601, 2008.

[50] Benjamin Texier and Kevin Zumbrun. Hopf bifurcation of viscous shock waves in compressible gas dynamics and mhd. *Arch. Ration. Mech. Anal.*, 190(1):107–140, 2008.

[51] Benjamin Texier and Kevin Zumbrun. Transition to longitudinal instability of detonation waves is generically associated with hopf bifurcation to time-periodic galloping solutions, 2008. Preprint.

[52] Forman A. Williams. *Combustion Theory*. Westview Press, 2 edition, 1985.

[53] Lung-An Ying. Finite difference method for a combustion model. *Math. Comp.*, 73(246):595–611 (electronic), 2004.

[54] Lung An Ying and Zhen Huan Teng. Riemann problem for a reacting and convection hyperbolic system. *Approx. Theory Appl.*, 1(1):95–122, 1984.

[55] Lung-an Ying, Tong Yang, and Changjiang Zhu. Nonlinear stability of strong detonation waves for a dissipative model. *J. Differential Equations*, 151(1):134–160, 1999.

[56] Lung-an Ying, Tong Yang, and Changjiang Zhu. The rate of asymptotic convergence of strong detonations for a model problem. *Japan J. Indust. Appl. Math.*, 16(3):467–487, 1999.

[57] Xin-ting Zhang and Lung-an Ying. Dependence of qualitative behavior of the numerical solutions on the ignition temperature for a combustion model. *J. Comput. Math.*, 23(4):337–350, 2005.

[58] Kevin Zumbrun. Stability of detonations in the ZND limit. *Arch. Ration. Mech. Anal.* to appear.

[59] Kevin Zumbrun and Peter Howard. Pointwise semigroup methods and stability of viscous shock waves. *Indiana Univ. Math. J.*, 47(3):741–871, 1998.